An Acad Bras Cienc (2022) 94(Suppl. 3): e20211352 DOI 10.1590/0001-3765202220211352
Anais da Academia Brasileira de Ciências | *Annals of the Brazilian Academy of Sciences*
Printed ISSN 0001-3765 I Online ISSN 1678-2690
www.scielo.br/aabc | www.fb.com/aabcjournal

GEOSCIENCES

Landslides associated with recent road constructions in the Río Lucma catchment, eastern Cordillera Blanca, Peru

ADAM EMMER, DANIEL HÖLBLING, LORENA ABAD, PETR ŠTĚPÁNEK, PAVEL ZAHRADNÍČEK & ILONA EMMEROVÁ

Abstract: Extensive road construction works recently took place in the remote eastern part of the Peruvian Cordillera Blanca, aiming at a better connection of isolated mountain communities with regional administrative centres. Here we document and characterize landslides associated with these road construction efforts in the Río Lucma catchment, Peru. We show that a total area of 321,332 m^2 has been affected by landslides along the 47.1 km of roads constructed between 2015 and 2018. While landslides downslope the roads (48.2%) and complex landslides crossing the roads (46.4%) were the most frequent landslide types in relation to the position of the road; slide-type movement (60.7%) prevails over the flow-type movement (39.3%). Timewise, we found that 75.0% of landslides were observed simultaneously with road construction work, while the remaining 25.0% occurred up to seven months after the roads had been constructed. We plotted the lagged occurrence of these subsequent landslides against precipitation data, showing that 85.7% of them were observed during the wet season (November to April). We conclude that the majority of mapped landslides were directly associated with road constructions and that the road constructions also may set preconditions for landslides, which mainly occurred during the subsequent wet season.

Key words: Cordillera Blanca, natural hazards, landslides, road construction, remote sensing, object-based image analysis (OBIA).

INTRODUCTION

Landslides are among the most common as well as the most researched natural hazards globally (Emmer 2018). They are particularly common in mountainous areas with high relief topography (Froude & Petley 2018, NASA 2020). In the Peruvian Andes, landslides claimed lives and caused tremendous infrastructure damages in the past (Evans et al. 2009, DesInventar 2019). The occurrence of landslides in the Peruvian Andes is often associated with increased precipitation during the wet season and El Niño forcing (Klimeš & Vilímek 2011, Vilímek et al. 2016), with earthquakes (Cluff 1971, Keefer 2002, Evans et al. 2009, Mergili et al. 2018b), or with glacier retreat and degrading permafrost (Klimeš et al. 2016, Haeberli et al. 2017, Emmer et al. 2020). Landslides in this region were also documented to initiate far-reaching process chains such as glacial lake outburst floods (GLOFs) (Emmer 2017, Mergili et al. 2018a).

Apart from natural triggers, also human activities are responsible or set preconditions for the occurrence of landslides across the globe. For instance, Gill & Malamud (2017) and Goudie (2020) listed many examples of human activities-driven acceleration of natural processes, preconditioning and triggering of

mass movements, including vegetation removal (Runyan & D'Odorico 2014, Pineda et al. 2016), loading additional weight onto slopes (Wang et al. 2011, 2020), changing groundwater conditions (Ho et al. 2013, Cigna et al. 2015), and excavating the base of the slopes (Stark et al. 2005, Peng et al. 2019).

Meeting most of these factors, landslides associated with road construction works in high mountain regions are frequently observed and have been a subject of scientific studies for decades (e.g. Swanson & Dryness 1975, Sidle et al. 2011) as well as recently (e.g. Sudmeier-Rieux et al. 2019, Taylor et al. 2020). Road construction works can also set preconditions for increased subsequent landslide activity, as, for example, described by McAdoo et al. (2018), who concluded that likely twice as many rainfall-triggered landslides occur in areas close to poorly constructed roads as it would be the case without roads. Information about the frequency and distribution of landslides along main roads is vital for better characterizing and understanding the impact that landslides may have on the population and assets in remote regions (Amatya et al. 2019). In the Peruvian Andes, such landslides are common, yet poorly documented and under-researched.

The main objectives of this study are: (i) to map and document landslides associated with road construction works in the Río Lucma catchment; (ii) to describe and explore different types of landslides, morphometrical statistics and the timing of occurrence in relation to road construction and season of the year. Combining these findings, we test the hypothesis that the road construction sets preconditions for slope movements, which are later on triggered by precipitations.

STUDY AREA

The Río Lucma catchment (77°22'-77°35' W, 8°53'-8°57' S; Fig. 1) is located on the eastern side of the Cordillera Blanca - the highest Peruvian mountain range - and covers an area of approximately 127 km^2. According to the 1:1,000,000 geological map of Peru (IGM 1975), the study area predominantly consists of sedimentary marine facies of Cretaceous age (Chicama and Lagunillas formations) with locally placed facies of continental origin. Plutonic rocks (Cordillera Blanca batholith) form the upper part of the valley. A NW-SE oriented fault runs through the middle part of the valley, being perpendicular to the valley streamline (parallel to the main Río Pomabamba valley). According to the nationwide mapping of susceptibility to mass movements (INGEMMET 2010), the susceptibility of the study area is ranked very high (the highest susceptibility class), referring to the occurrence of slopes with fault zones, masses of intensely weathered, saturated and highly fractured rocks with unfavourable discontinuities, and unconsolidated deposits.

The Río Lucma flows in roughly west-to-east direction and is the right-sided tributary of the Río Pomabamba, which is a part of the Río Marañón (Amazon) basin. The closest SENAMHI (Servicio Nacional de Meteorología e Hidrología del Perú) hydrometeorological stations are located in Pomabamba and Piscobamba, i.e. approximately 9 km and 4 km away from the Río Lucma catchment, respectively. The stations have an average rainfall of 1,169 mm/year, 80% of it corresponding to the wet or rainy season (i.e. November to April). The very upper parts of the catchment are covered by glaciers (Taulliraju, 5,830 m a.s.l.) and form a part of the Huascarán National Park, while the lowest point is the confluence of the Río Lucma with the Río Pomabamba (2,500 m a.s.l.). The elevation

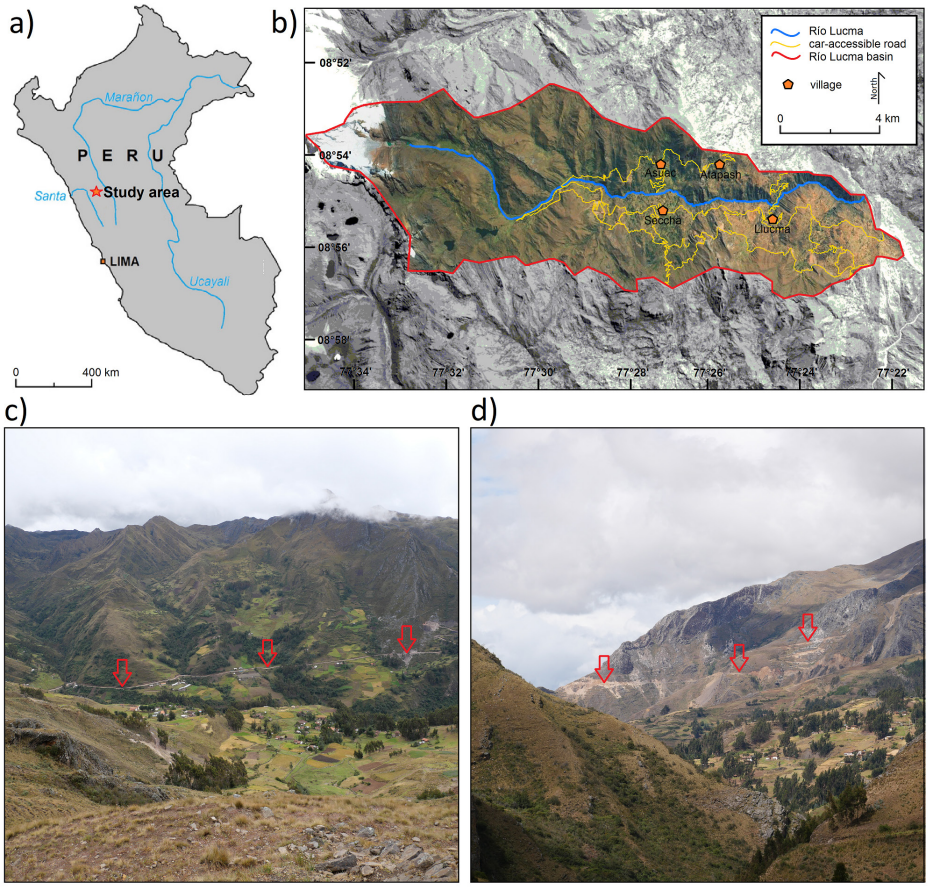

Figure 1. The study area of the Río Lucma catchment. a) shows the location of the study area in Peru; b) shows the Río Lucma catchment, the road network (as of June 2018) and the location of the main villages; c) shows a view into the middle part of the Río Lucma valley (red arrows highlight recently constructed roads); d) shows a view to the east of the study area (red arrows highlight recently constructed roads).

difference of more than 3,300 m in combination with the lithological and structural geological settings make this area generally susceptible to gravitational mass movements, with numerous historical as well as recent landslides observable in the field. One of the largest ancient landslides dammed the Lake Huacrucocha, located in the middle part of the valley (Tacconi-Stefanelli et al. 2018).

The northern part of the Río Lucma basin belongs to the Pomabamba administrative district, while the southern part belongs to the Mariscal Luzuriaga administrative district, Ancash region. Apart from the largest village, Lucma, several small villages (e.g. Asuac, Atapac, Seccha) and numerous farms and single houses are located within the catchment (see Fig. 1) up to an elevation of about 4,000 m a.s.l. Many of these remote settlements - especially those located in the middle and upper part of the valley - are still not accessible by car today. Recent development efforts, however, have resulted in a construction 'boom' in the study area since early 2010s. Predominantly, simple unpaved roads have been constructed in order to connect these settlements to each other as well as to larger regional centers such as Lucma and Pomabamba. Despite being located in a high relief landslide-prone area, these roads are rarely equipped with any kind of drainage or landslide mitigation measures.

MATERIALS AND METHODS

Data and analysis workflow

The workflow of this study consists of several consecutive steps and a two-level analysis: (i) a detailed analysis in three areas of interest

(AOIs), i.e. parts of the whole study area selected due to the high concentration of landslides; and (ii) a wider analysis covering the whole study area. Landslides within the three AOIs were manually mapped (see Manual landslide mapping), described in detail and analyzed in relation to rainfall data (see Rainfall data analysis). A visual inspection of daily satellite imagery was performed to estimate the date of landslide occurrence. For mapping landslides in the whole study area, we employed a semi-automated OBIA approach and assessed its performance (see Object-based image analysis (OBIA) for landslide mapping).

In this study, we integrated field data and satellite images to manually and semi-automatically map the landslides. A field survey was performed in June 2019, aiming at reconnaissance, mapping and photo documentation of landslides along recently constructed roads in the study area with a special focus on three AOIs. We used very high resolution (VHR) remotely sensed optical images available in Google Earth Pro (Google Inc. 2022) and multispectral PlanetScope and RapidEye-2 images from Planet Labs Inc. (Planet Team 2019), covering the time period from June 2015 to July 2018. The remote sensing data used for semi-automated landslide identification with object-based image analysis (OBIA) are listed in Table I. In addition to multispectral imagery, the ALOS PALSAR DEM with 12.5 m resolution (ASF DAAC 2015) and the derived slope were used as ancillary data for landslide detection.

Manual landslide mapping

First, we used recent VHR images available in Google Earth (image acquisition in July 2018) to manually map the complete road network, since no up-to-date map is publicly available at the date of the study. We used QGIS Version 3.10 A Coruña – a free and open source geographic information system (https://qgis.org/) – for the mapping. Subsequently, the sections of roads which have been constructed since 2015 were identified. Then, three AOIs were defined, in which we manually mapped landslides associated with road construction efforts. For this step, the visual interpretation of VHR images was combined with field documentation. We described manually delimited landslides by several quantitative characteristics, e.g. area, elevation of the headscarp and deposition, reach (in m and in °), and qualitative characteristics, e.g. movement type (flow vs. slide), type of release and deposition zone in relation to the road location (Fig. 2), etc. Movement type is distinguished based on the morphometrical characteristics of mapped landslides (flow-type movement is defined as prolong-shaped landslide with length to width ratio > 3; see Table II). A complete list of characteristics assigned to each landslide within the three AOIs is shown in Table II. Among the other characteristics, the timing of occurrence (i.e. the period between

Table I. Remote sensing data used for semi-automated landslide identification.

Sensor	Acquisition Date	Spatial Resolution	Bands/Beam Mode
RapidEye-2	21.06.2015	5 meters	Red, Green, Blue, Red Edge, Near Infrared
PlanetScope	01.10.2017	3 meters	Red, Green, Blue, Near Infrared
	28.07.2018		
ALOS-1 PALSAR RTC	20.10.2010	12.5 meters	Fine Beam Dual Polarization (FBD)

road construction and landslide occurrence) was determined for each landslide, based on the visual inspection of daily scenes of VHR imagery available on the Planet Explorer online tool. The daily scenes included imagery between January 2017 and July 2018. We compared results of manual mapping to OBIA results in the three AOIs (see Object-based image analysis (OBIA) for landslide mapping). The manual mapping served as reference data. Producer's and user's accuracies were calculated based on the amount of overlapping area between the classifications.

Object-based image analysis (OBIA) for landslide mapping

OBIA has been successfully used for the identification of land surface changes and landslides in diverse geographical settings (e.g. Lahousse et al. 2011, Stumpf & Kerle 2011, Hölbling et al. 2012, 2015, 2016a, 2017, Martha et al. 2012, Heleno et al. 2016, Amatya et al. 2019). OBIA provides a set of advanced tools for semi-automated landslide detection based on remote sensing data, relying on the concepts of image segmentation and classification and allowing the use of a range of spectral, spatial, textural and contextual properties of image objects during the classification process (e.g. Blaschke et al. 2014, Hölbling et al. 2017).

We employed OBIA to semi-automatically map the landslides next to roads in the whole study area using the eCognition (Trimble) software. We applied the multiresolution segmentation algorithm (Baatz & Schäpe 2000), a bottom-up region merging technique, to create image objects that served as a basis for the classification. Segmentation was performed individually on the PlanetScope images from 01.10.2017 and 28.07.2018, while the same bands (red, green, blue, near-infrared) and parameters (scale parameter: 400; shape: 0.6; compactness: 0.1) were used. The parameters and thresholds for segmentation and classification were determined based on expert knowledge and visual assessment. For the detection of landslides caused by road construction, we considered changes in the values of spectral indices (i.e. Normalized Difference Vegetation Index (NDVI), Modified Soil-adjusted Vegetation Index (MSAVI), brightness) per image object between RapidEye-2 from 21.06.2015 and PlanetScope from 01.10.2017 and between the two PlanetScope images from 01.10.2017 and 28.07.2018, respectively. New landslides appear brighter and show relatively low NDVI and MSAVI values, thus, landslide

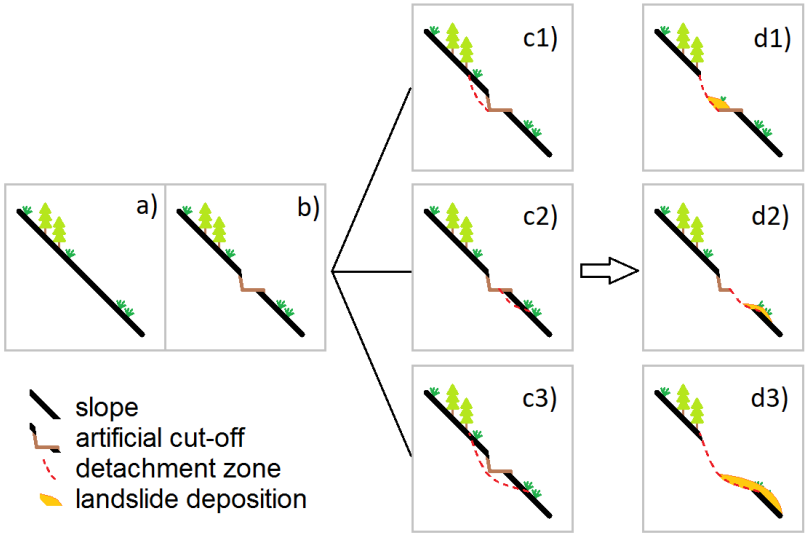

Figure 2. Schematic types of release and deposition zones (in relation to the road location) distinguished in this study. a) shows the initial state before the construction of the road and b) shows the initial state after the construction of the road; c) shows pre-failure conditions and d) shows post-failure states. Landslides onto the road (1), landslides downslope the road (2) and complex landslides (3) are distinguished.

candidates could be classified accordingly. While the same classification parameters were applied for mapping landslides based on the 2017 and 2018 images, the thresholds were slightly adapted due to the different acquisition times and because new landslides in 2017 were identified by comparing images from different satellite sensors. By additionally using a slope threshold of > 15 ° and considering contextual characteristics (i.e. overlap of landslide and road features), the semi-automated classification was refined, and only landslides next to roads were identified. Finally, after merging the classified landslide objects, small (<150 m^2) features were eliminated. Following this approach, we were able to identify the landslides triggered by road construction during two periods: from June 2015 to September 2017 and from October 2017 to July 2018.

Rainfall data analysis

We acquired, processed and analyzed daily rainfall data for the "POMABAMBA" and "PISCOBAMBA II" SENAMHI stations to reveal the possible relationship between rainfall and the occurrence of landslides. While these stations are not located directly in the Lucma catchment but within a distance of 4 and 9 km, respectively, data from these two stations were the best available. The rainfall data from both stations were used to determine wet and dry periods. Additionally, we calculated daily rainfall on the day of landslide occurrence, and cumulative rainfall (for 3, 5, 10, 14, and 30 days) before landslide occurrence, for each manually delineated landslide. The temporal coverage of the rainfall data did not cover the study period for the "PISCOBAMBA II" station and therefore only daily rainfall from "POMABAMBA" was used

Table II. Attributes assigned to each of the manually identified landslides in the three areas of interest.

Attribute	Description	Units	Data
Location	Longitude and latitude of the centroid of the landslide	°S; °W	Derived automatically
Head scarp elevation	The elevation of the highest point of the landslide	m a.s.l.	Derived automatically
Deposition elevation	The elevation of the lowest point of the landslide	m a.s.l.	Derived automatically
Area affected	Area affected by the landslide (including detachment, transport and deposition zones)	m^2	Derived automatically
Reach (m)	A distance between the head scarp and the lowest reach of landslide deposition	m	Derived automatically
Vertical difference	Vertical difference between the head scarp elevation and the elevation of the lowest reach of landslide deposition (Deposition elevation)	m	Derived automatically
Reach (°)	A mean slope calculated from Vertical difference and Reach (m)	°	Calculated automatically
Type	Distinction between 'flow' and 'slide' type*	-	Assigned manually
Release and deposition zone (in relation to road location)	Distinction between: (i) landslide onto the road; (ii) landslide downslope the road; and (iii) complex landslide (see Fig. 2)	-	Assigned manually
Occurrence	Time period between the closest pre- and post-landslide images	Date range	Assigned manually
Timing of occurrence	Time period between road construction and the occurrence of landslides	Days	Assigned manually

*** - flow type landslide is defined as a landslide where the length to width ratio is > 3.**

for this analysis. These rainfall values were analyzed according to the time of occurrence of the landslide (i.e. whether the landslide and the new road had been observed at the same time, or the landslide was observed after new road construction), and the statistical differences were evaluated using a nonparametric Wilcoxon rank-sum test (significance level: 5%; Helsel & Hirsch 1993). The nonparametric Wilcoxon rank-sum test was used because the data did not follow a normal distribution. We also referred to the Coastal El Niño Index (ICEN) to determine the El Niño–Southern Oscillation (ENSO) phase. The ICEN is a 3-month running mean of sea temperature anomalies on the Niño 1+2 region, which is commonly used to determine ENSO phases for the Peruvian coast (Takahashi et al. 2014).

RESULTS

Landslides along the recently constructed roads in the Río Lucma catchment

Field morphological evidence corroborates that the Río Lucma catchment has been a subject of landsliding in the past. In this work, we show that many recent landslides are associated with the road construction efforts taking place in the region (see examples in Fig. 3). A total of 105.8 km of car-accessible roads was mapped in the Río Lucma catchment (as of June 2018), of which 47.1 km (44.5%) have been constructed since June 2015. A total of 56 landslides with a total area of 321,332 m^2 have been mapped (see Table SI – Supplementary Material) along the newly constructed road sections (i.e. road sections constructed since June 2015). The area of individual landslides (including detachment, transport, and depositional zone) varies from 248 m^2 (ID_42) to 40,587 m^2 (ID_56), while the

Figure 3. Examples of landslides associated with recent road construction works in the Río Lucma catchment. a) shows several landslides onto the newly constructed road near Asuac (AOI_3); note the detail of the landslide-prone structural-geological setting. These landslides are interpreted as partial reactivations of larger complex slope deformation in this area. b) shows a crack and detached part of the road which is likely to fail (landslide downslope the road) near the Niño Rajra bridge; typical landslide-prone, nearly vertical up to 10 m high, non-mitigated slopes formed by unstable sediments are captured in the left part of the image. c) shows two landslides affecting parts of newly constructed roads on the northern side of the Lucma river (AOI_3). d) shows a downslope view on a recently constructed road section and deposition area of a flow-type movement in AOI_2. All images were taken by Adam Emmer in June 2019.

average size is 5,738 m^2 and the medium size 3,030 m^2. The head scarps (detachment zones) are located at elevations ranging from 3,670 m a.s.l. (ID_41) to 3,948 m a.s.l. (ID_16) and the depositions are located in between 3,545 m a.s.l. (ID_43) and 3,876 m a.s.l. (ID_15).

Landslides downslope the roads were the most frequent (48.2%), followed by complex landslides (starting above the road and continuing downslope the road; 46.4%) while three landslides (5.4%) are characterized as landslides onto the road. While landslides onto the road are interpreted to occur in association with the excavation of the base of the slope, landslides downslope the road are interpreted to occur in association with increased load and shaking induced by passing cars, and possibly with changed soil moisture conditions (increased water infiltration into the slope due to rainfall; see Occurrence of landslides in relation to road construction and rainfall in three AOIs). As for the movement types, we classify 60.7% of detected landslides as slides and 39.3% as flows. Some of the landslides are thought to occur as a result of partial reactivation of slope movements in areas of existing complex slope deformations (see Fig. 3a).

By using OBIA, we successfully identified 47 out of the 56 manually mapped landslides in the three AOIs, with 20 out of 29 in AOI_1, 11 out of 11 landslides identified in AOI_2 and 16 out of 16 landslides in AOI_3 (see Table III). When comparing the overlapping area, the overall producer's accuracy is 60.5%, varying from 49.0% (AOI_3) to 87.8% (AOI_2) and the overall user's accuracy is 49.5 %, varying from 42.5% (AOI_2) to 64.4% (AOI_3). By analyzing the the whole study area with OBIA, we identified a total area of 882,459 m^2 affected by landslides associated with recent road constructions (see Fig. 4), whereby 583,137 m^2 were mapped on the 2017 PlanetScope image, i.e. new landslides compared to the RapidEye image from 2015, and 299,322 m^2 were mapped on the 2018 PlanetScope image, i.e. new landslides compared to the PlanetScope image from 2017. By July 2018, 14.3 km (i.e. approximately 30%) of the newly constructed roads have been affected by landslides in the whole study area.

Occurrence of landslides in relation to road construction and rainfall in three AOIs

During visual inspection of daily VHR PlanetScope imagery in the Planet Explore online platform for each of the 56 manually delimited landslides, we observed in 42 cases (75.0%) that the landslide and the newly constructed road appear for the first time in the same VHR image, which implies that they likely occurred on the same day or immediately

Table III. Comparison of object-based image analysis (OBIA) and manual mapping results per area of interest (AOI) and accuracy values.

	AOI 1	AOI 2	AOI 3	Overall
OBIA mapping (m^2)	174,024	115,299	102,609	**391,932**
Manual mapping (m^2)	130,546	55,845	134,940	**321,332**
Difference OBIA - Manual mapping (%)	33.30	106.46	-23.96	**21.97**
Overlap area (m^2)	79,220	49,034	66,109	**194,363**
Producer's accuracy (%)	60.68	87.80	48.99	**60.49**
User's accuracy (%)	45.52	42.53	64.43	**49.59**
Manual mapping (No. of landslides)	29	11	16	**56**
No. of manually mapped landslides coinciding with OBIA mapping	20	11	16	**47**

after the road construction. However, due to the identical morphological appearance, we cannot completely exclude the possibility that some of the downslope deposited landslides, which are observed to occur immediately after the road construction, are downslope depositions of surplus material removed and deposited by the workers during the construction works.

For the remaining 14 cases (25.0%), two landslides (3.6%) were identified in imagery acquired within one week after the road construction was observed, four (7.1%) within two to four weeks, and eight (14.3%) between two and seven months after the road construction (see Fig. 5). Road construction seemed to be a preconditioning factor for the triggering of these landslides, however, their exact trigger is difficult to determine. We attempted to link the occurrence of these 14 landslides with rainfall accumulation interpolated for each landslide location, however, the available data from two nearby-located meteorological stations were not sufficient to perform a reliable local interpolation of rainfall for the study area. Nevertheless, the information from the meteorological stations allowed us to conclude that 12 landslides occurred during the wet season (November to April), while only two occurred during the dry season (May to October). Based on the ICEN, the period between November 2017 and March 2018 presented an ENSO strong cool phase or "La Niña" period. "La Niña" is associated with higher precipitation in the higher mountains (Vuille & Keimig 2004, Romero et al. 2007). During this

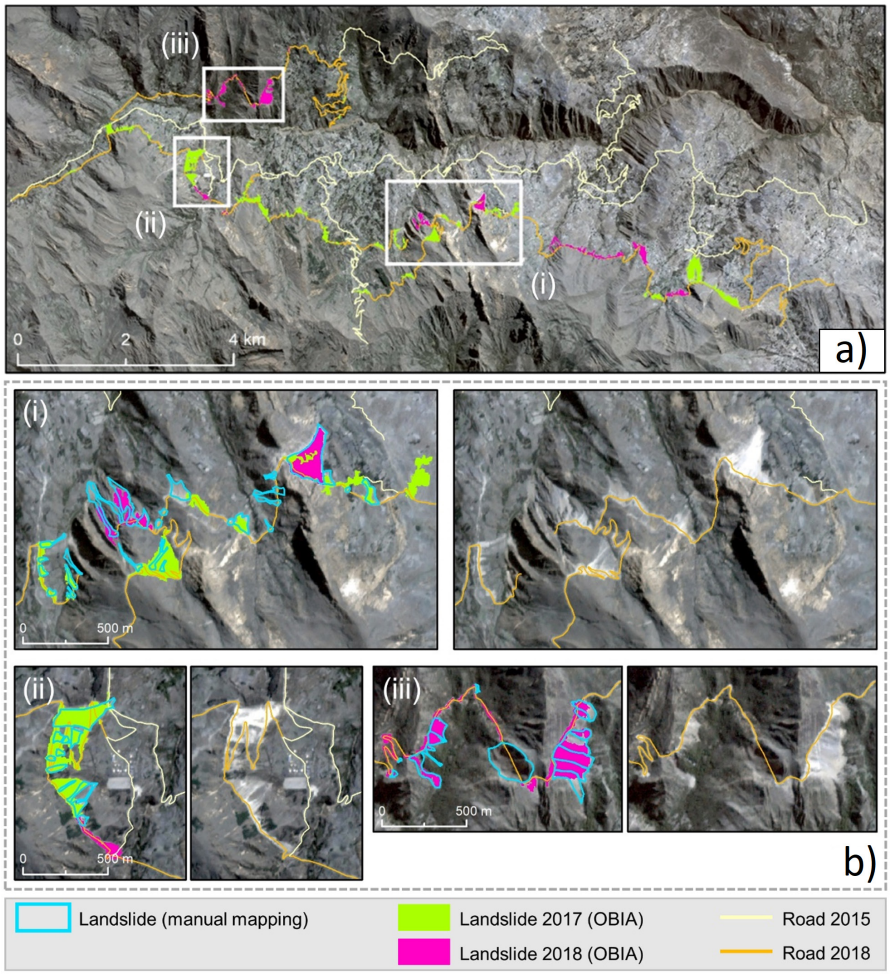

Figure 4. Mapped landslides along the recently constructed roads. a) shows the landslides mapped with OBIA in the whole study area and indicates the location of the three AOIs. The PlanetScope image from 28.07.2018 is shown in the background. b) shows the manual and OBIA mapping results in the three AOIs ((i), (ii), (iii)) and the PlanetScope image from 28.07.2018.

time, road construction progressed significantly, leading to 23 (41.1%) of the observed landslides. Ten of them (17.9%) were observed between one week and five months after road construction.

Fig. 6 indicates the relationship between daily rainfall registered at the "POMABAMBA" station and cumulative rainfall for landslides observed at the same time as the road was constructed, and for landslides detected after road construction. Daily rainfall registered on the day of landslide occurrence does not show significant differences between landslides observed concurrently to road construction, and those observed after the road had been constructed (Fig. 6a). This implies that landslides observed at the same time as road construction were actually triggered by these works. Likewise, there is no significant difference between cumulative rainfall registered 3, 5, 10, and 30 days before landslide occurrence when comparing the landslides observed during and after road construction. Only cumulative rainfall 14 days

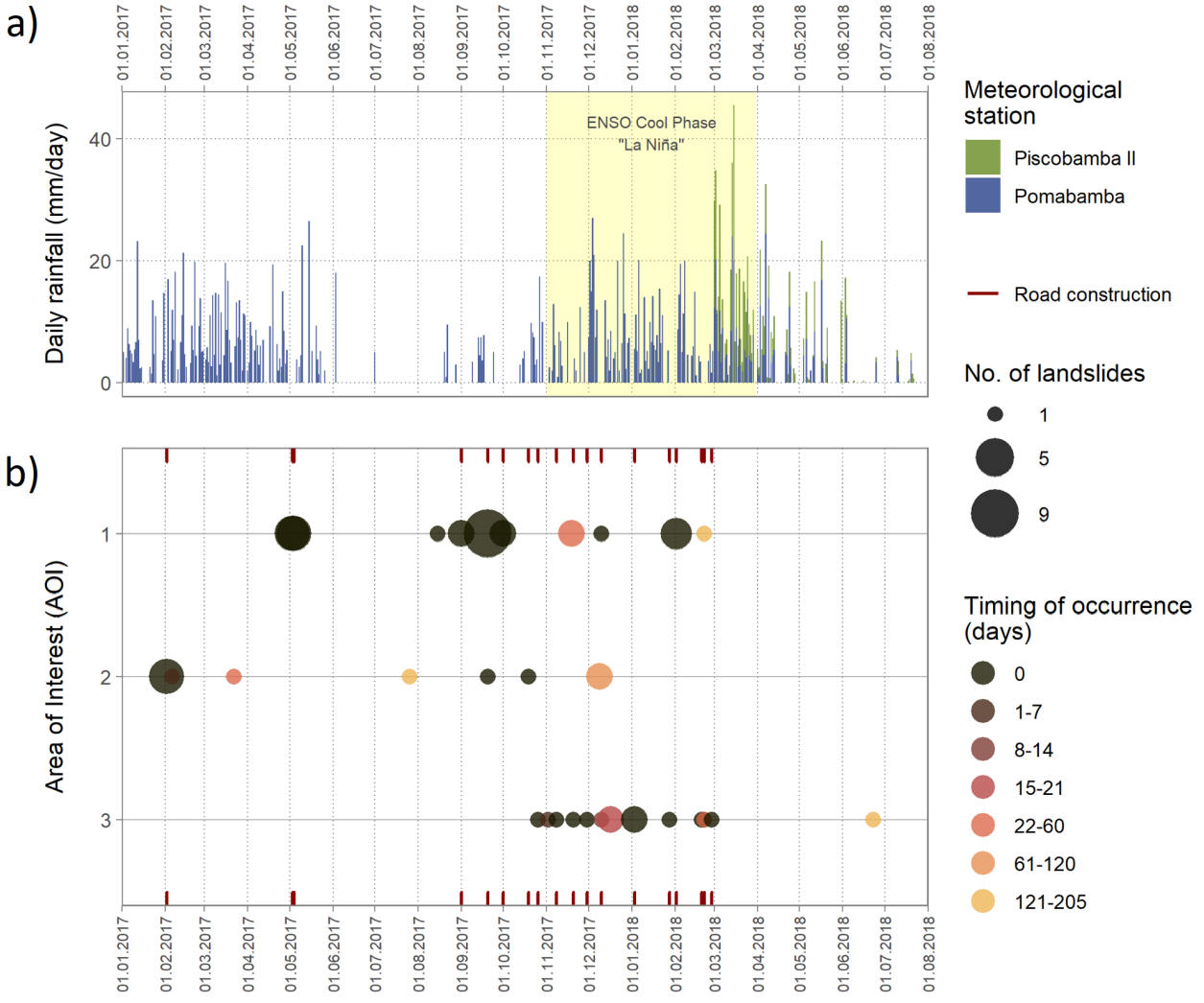

Figure 5. Rainfall and the occurrence of landslides in the three AOIs. **a)** indicates the daily rainfall recorded by the two closest SENAMHI meteorological stations, the ENSO Cool Phase "La Niña" period is highlighted in yellow. **b)** indicates the occurrence of landslides per AOI. The size of the circle represents the number of landslides, while the colour represents the time difference between landslide occurrence and road construction. The landslide occurrence and road construction dates refer to the first time the landslide or the new road, respectively, was observed on VHR imagery. Road construction dates are marked at the top and bottom of the graph.

before the landslide occurrence seems to be higher (statistically significant with a p-value < 0.05) for those landslides registered after road construction (Fig. 6e). Thus, we infer that a two-week cumulative rainfall might have triggered these landslides. It is worth noting that the landslide occurrence day refers to the first time the landslide was observed on VHR imagery, hence, this analysis should be interpreted with care. In addition, other factors like soil saturation and dry spells could influence the occurrence of landslides, however, the two meteorological stations did not provide enough information to derive such parameters.

DISCUSSION

OBIA vs. manual mapping of landslides

Visual interpretation of aerial or satellite images and manual mapping of landslides is generally more accurate than semi-automated methods, but it is a very time-consuming process. Any mapping task for large areas would likely benefit from a degree of automation with the potential to reduce the time and effort for creating landslide maps (Hölbling et al. 2016a, b). Thus, we decided to manually map landslides next to roads in three identified focus areas, and then to perform a large-scale mapping by employing an OBIA approach.

Visual interpretation shows advantages over OBIA for delineating single landslides and for splitting up compound landslide complexes

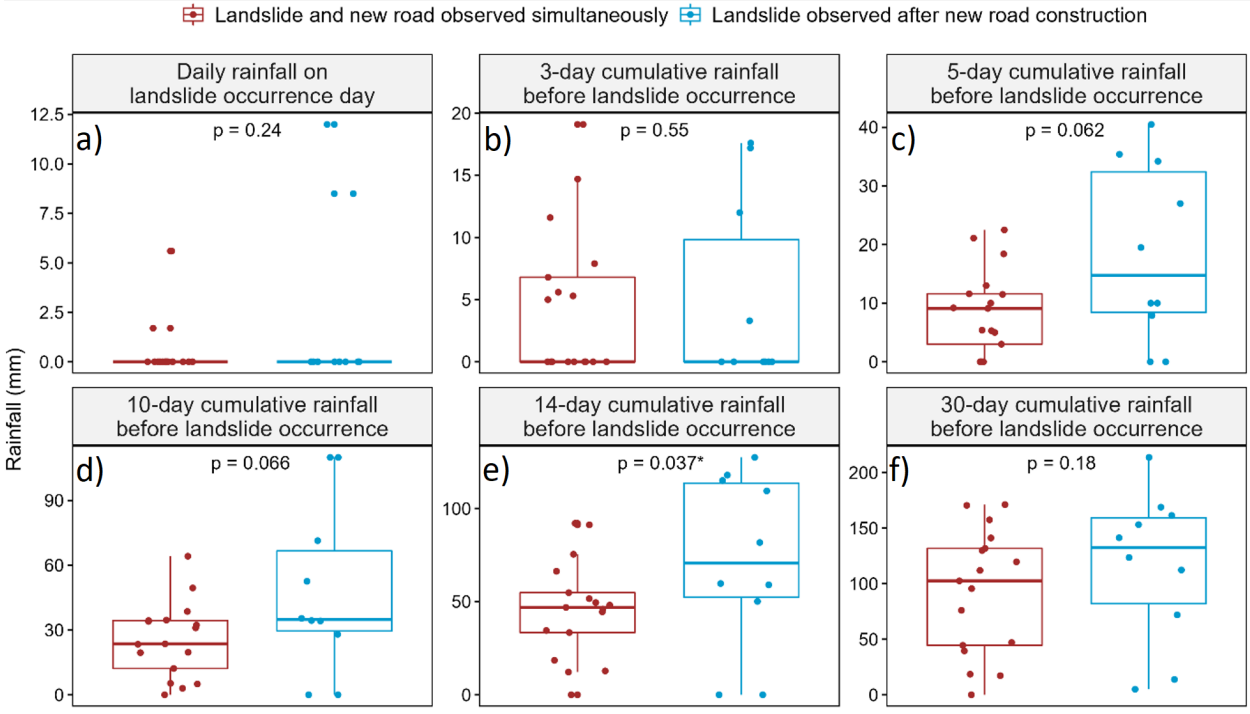

Figure 6. Daily rainfall and cumulative rainfall relation for landslides and road construction observed simultaneously and landslides observed after the new road construction. a) shows the difference per group for the daily rainfall on the day of landslide occurrence, b) for the 3-day cumulative rainfall before landslide occurrence, c) for 5-day cumulative rainfall, d) for 10-day cumulative rainfall, e) 14-day cumulative rainfall, and f) for 30-day cumulative rainfall. The p-value indicates the significance level of the Wilcoxon rank-sum test (p-value < 5% marked with *). The landslide occurrence and road construction dates refer to the first time the landslide or the new road, respectively, was observed on VHR imagery.

into separate landslides (Hölbling et al. 2016a), as well as for deriving qualitative characteristics. Manual mapping allowed us to identify the number of landslides in the focus areas and to interpret and classify them according to movement types. The expert knowledge needed for deriving such information is difficult to implement in automated mapping workflows.

The accuracy of our OBIA landslide mapping is acceptable but moderate in terms of the overlap area. It is important to mention that additional data sources (Google Earth Pro imagery, field documentation) were considered for manual mapping compared to the OBIA mapping. This probably influences the accuracy values. However, we were able to successfully detect the majority of landslides in the three focus areas. Thus, we applied OBIA to map landslides in the whole study area. Despite the limitations of the semi-automated method, such as the potential concurrent identification of natural (e.g. landslides) and man-made changes (e.g. constructions) due to similar spectral properties, it is faster and more transparent than manual mapping. Some problems in the OBIA mapping can be associated with shadow areas, which did not allow to semi-automatically detect all new landslides since no significant spectral changes associated with landslide activity could be identified (see, for example, the large complex landslide in AOI (iii) in Fig. 4b that was mapped manually but missed using OBIA).

The OBIA results for the whole Lucma area give a good overview of road sections that have been predominantly affected by landslides. Providing information about landslides affecting roads over large areas can be helpful to support the targeted planning of road maintenance and reconstruction efforts. Moreover, since the OBIA results can be produced quickly, they might be particularly valuable for rapid information provision.

Damages caused, landslide mitigation and post-landslide recovery

Landslides associated with road constructions usually do not directly cause fatalities or extreme infrastructure damages, considering their magnitude, dynamics and the sporadic presence of tangible assets in the study area. Most of the damages are, therefore, related to the roads themselves. However, landslide-associated disruptions of the road infrastructure network may cause secondary impacts such as goods supply problems and the limited ability of inhabitants to travel for work, educational or medical purposes.

The roads in the study area are mainly designed and built without any landslide mitigation measures (see Fig. 3b). On the other hand, such constructions are fast, cheap and easy to repair at the same time. Since there is no option to take a detour of a landslide-affected road, maintenance and repair actions have to take place immediately. During the field campaign, we eye-witnessed spontaneous post-landslide recovery actions. In case of a landslide onto the road, the deposited material was removed using manpower (for smaller depositions) or heavy machinery in case of larger depositions. In the case of a landslide downslope the road, a narrowed part of the road was simply widened by further excavation of the base of the slope. In exceptional cases of complex and large landslides, alternative road sections have been built at several locations to bypass landslide-affected areas (see the example of the unfinished road section in AOI_3 which was severely affected by landslides, so that it had to be bypassed, Fig. 7).

In general, we observed that the majority of mapped landslides are directly (e.g. landslides resulting from slope undercutting) or indirectly associated with road constructions (e.g. rainfall-induced landslides resulting from a combination

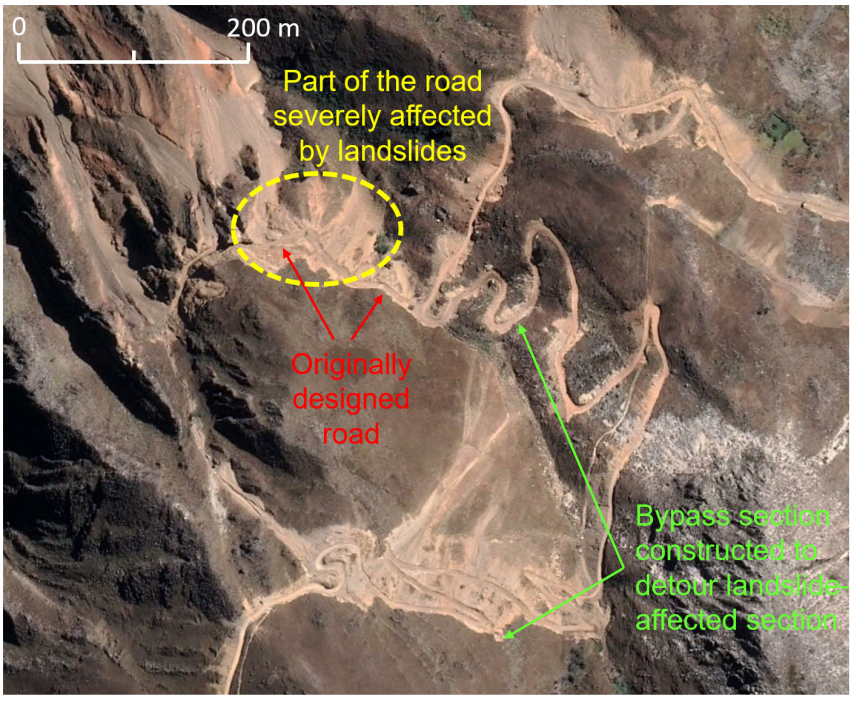

Figure 7. Aerial view of a subpart of AOI_1 with an example of a road constructed to bypass a road section affected by landslides. Image: CNES / Airbus, 22.6.2018 (available from Google Earth collection; Google Inc. 2022).

of extreme precipitation over slopes with decreased stability). It is likely that construction work also sets a precondition for rainfall-induced landslides in the Río Lucma catchment, however, further investigations and additional data would be needed to prove this assumption rigorously. Two-week cumulative rainfall and "La Niña" cool-phase seemed to have an influence on the number of landslides triggered after road construction, which matches observations from other Andean regions (Naranjo Bedoya et al. 2019).

CONCLUSIONS

Our study demonstrates how road construction efforts that took place in the high mountain Río Lucma catchment in the Peruvian Cordillera Blanca are associated with numerous landslides. Our findings reveal a fast reaction of slopes to this anthropogenic forcing, with most of the landslides occurring during or immediately after the road construction. Our observations corroborate that a considerable number of new landslides may be associated with road constructions in landslide-prone areas and partial reactivations of existing landslide complexes on the one hand (see Fig. 3a) and the absence of any landslide mitigation measures along with road construction on the other hand (see Fig. 3b). While road construction in this geographical environment and socioeconomic context is undoubtedly a challenging task, better understanding mechanisms, timing and processes behind the occurrence of landslides may help to outline enhanced risk reduction and sustainable development strategies.

Acknowledgments

We would like to express our thanks to two anonymous reviewers who provided valuable comments and suggestions which helped us to shape this study. This work was initially supported by the AUT-CZE MOBILITY project 'Is the occurrence of slope movements in the Cordillera Blanca, Peru, influenced by the El Niño Southern Oscillation?' (Project No. 8J18AT032 and CZ 04/2018, respectively). DH and LA have also been supported by the Austrian Research Promotion Agency (FFG) through the project MontEO (The impact of mass movements on alpine trails and huts assessed by EO

data; contract no. 873667). All data generated in this study (mapping results) are included in this published article and its supplementary information files.

REFERENCES

AMATYA P, KIRSCHBAUM D & STANLEY T. 2019. Use of Very High-Resolution Optical Data for Landslide Mapping and Susceptibility Analysis along the Karnali Highway, Nepal. Remote Sens 11(19): 2284.

ASF DAAC. 2015. ALOS-1 PALSAR Radiometric Terrain Corrected high resolution; Includes Material © JAXA/METI 2010. 10.5067/Z97HFCNKR6VA.

BAATZ M & SCHÄPE A. 2000. Multiresolution Segmentation: An optimization approach for high quality multi-scale image segmentation. In: Strobl J, Blaschke T & Griesebner G (Eds), Angewandte Geographische Informationsverarbeitung XII; Wichmann: Berlin/Heidelberg, Germany, p. 12-23.

BLASCHKE T, FEIZIZADEH B & HÖLBLING D. 2014. Object-Based Image Analysis and Digital Terrain Analysis for Locating Landslides in the Urmia Lake Basin, Iran. IEEE J Sel Top Appl Earth Obs Remote Sens 7(12): 4806-4817.

CIGNA F, JORDAN H, BATESON L, MCCORMACK H & ROBERTS C. 2015. Natural and Anthropogenic Geohazards in Greater London Observed from Geological and ERS-1/2 and ENVISAT Persistent Scatterers Ground Motion Data: Results from the EC FP7-SPACE PanGeo Project. Pure Appl Geophys 172(11): 2965-2995.

CLUFF LS. 1971. Peru earthquake of May 31, 1970, engineering geology observations. Bull Seismol Soc Am 61: 511-533.

DESINVENTAR. 2019. Inventory system of the effects of disasters. URL:< https://www.desinventar.org/>; Accessed: August 2019.

EMMER A. 2017. Geomorphologically effective floods from moraine-dammed lakes in the Cordillera Blanca, Peru. Quat Sci Rev 177: 220-234.

EMMER A. 2018. Geographies and Scientometrics of Research on Natural Hazards. Geosciences 8(10): 382.

EMMER A, KLIMEŠ J, HÖLBLING D, ABAD L, DRAEBING D, SKALÁK P, ŠTĚPÁNEK P & ZAHRADNÍČEK P. 2020. Distinct types of landslides associated with the post-LIA glacier thinning: observations from the Kinzl glacier, Huascarán, Peru. Sci Total Environ 739: 139997.

EVANS SG, BISHOP NF, FIDEL SMOLL L, VALDERRAMA MURILLO P, DELANEY KB & OLIVER-SMITH A. 2009. A re-examination of the mechanism and human impact of catastrophic mass flows originating on Nevado Huascarán, Cordillera Blanca, Peru in 1962 and 1970. Eng Geol 108: 96-118.

FROUDE MJ & PETLEY DN. 2018. Global fatal landslide occurrence from 2004 to 2016. Nat Hazards Earth Syst Sci 18: 2161-2181.

GILL JC & MALAMUD BD. 2017. Anthropogenic processes, natural hazards, and interactions in a multi-hazard framework. Earth Sci Rev 166: 246-269.

GOOGLE INC. 2022. Google Earth Pro, v.7.1.5.1557.

GOUDIE A. 2020. The human impact in geomorphology – 50 years of change. Geomorphology 366: 106601.

HAEBERLI W, SCHAUB Y & HUGGEL C. 2017. Increasing risks related to landslides from degrading permafrost into new lakes in de-glaciating mountain ranges. Geomorphology 293(B): 405-417.

HELENO S, MATIAS M, PINA P & SOUSA AJ. 2016. Semiautomated object-based classification of rain-induced landslides with VHR multispectral images on Madeira Island. Nat Hazards Earth Syst Sci 16: 1035-1048.

HELSEL DR & HIRSCH RM. 1993. Statistical Methods in Water Resources. In Studies in Environmental Science 49. Amsterdam: Elsevier Science, 522 p.

HO KKS, CHAO PA, LAU TMF & DE SILVA S. 2013. Investigation of the 20 August 2005 fatal landslide at Fu Yung Shan Tsuen, Hong Kong. Landslides 10(3): 285-297.

HÖLBLING D, BETTS H, SPIEKERMANN R & PHILLIPS C. 2016a. Identifying Spatio-Temporal Landslide Hotspots on North Island, New Zealand, by Analyzing Historical and Recent Aerial Photography. Geosciences 6: 48.

HÖLBLING D, BETTS H, SPIEKERMANN R & PHILLIPS C. 2016b. Semi-automated landslide mapping from historical and recent aerial photography. In Proceedings of the 19th Agile 2016 Conference on Geographic Information Science, Helsinki, Finland, 14-17 June, p. 5.

HÖLBLING D, EISANK C, ALBRECHT F, VECCHIOTTI F, FRIEDL B, WEINKE E & KOCIU A. 2017. Comparing Manual and Semi-Automated Landslide Mapping Based on Optical Satellite Images from Different Sensors. Geosciences 7(2): 37.

HÖLBLING D, FRIEDL B & EISANK C. 2015. An object-based approach for semi-automated landslide change detection and attribution of changes to landslide classes in northern Taiwan. Earth Sci Inform 8(2): 327-335.

HÖLBLING D, FÜREDER P, ANTOLINI F, CIGNA F, CASAGLI N & LANG S. 2012. A Semi-Automated Object-Based Approach for Landslide Detection Validated by Persistent Scatterer

Interferometry Measures and Landslide Inventories. Remote Sens 4(5): 1310-1336.

IGM. 1975. Mapa geologico del Peru 1:1,000,000. Instituto de Geologia y Mineria (IGM), 1 p.

INGEMMET. 2010. Mapa de susceptibilidad por movimientos en masa de Perú 1:2,000,000. Instituto Geológico Minero y Metalúrgico (INGEMMET), 1 p.

KEEFER DK. 2002. Investigating landslides caused by earthquakes - A historical review. Surv Geophys 23(6): 473-510.

KLIMEŠ J ET AL. 2016. Landslides in moraines as triggers of glacial lake outburst foods: example from Palcacocha Lake (Cordillera Blanca, Peru). Landslides 13(6): 1461-1477.

KLIMEŠ J & VILÍMEK V. 2011. A catastrophic landslide near Rampac Grande in the Cordillera Negra, northern Peru. Landslides 8(3): 309-320.

LAHOUSSE T, CHANG KT & LIN YH. 2011. Landslide mapping with multi-scale object-based image analysis – a case study in the Baichi watershed, Taiwan. Nat Hazards Earth Syst Sci 11: 2715-2726.

MARTHA TR, KERLE N, VAN WESTEN CJ, JETTEN V & KUMAR KV. 2012. Object-oriented analysis of multi-temporal panchromatic images for creation of historical landslide inventories. ISPRS J Photogramm Remote Sens 67: 105-119.

MCADOO BG, QUAK M, GNYAWALI KR, ADHIKARI BR, DEVKOTA S, RAJBHANDARI PL & SUDMEIER-RIEUX K. 2018. Roads and landslides in Nepal: how development affects environmental risk. Nat Hazards Earth Syst Sci 18: 3203-3210.

MERGILI M, EMMER A, JUŘICOVÁ A, COCHACHIN A, FISCHER JT, HUGGEL C & PUDASAINI SP. 2018a. How well can we simulate complex hydro-geomorphic process chains? The 2012 multi-lake outburst flood in the Santa Cruz Valley (Cordillera Blanca, Perú). Earth Surf Process Landf 43(7): 1373-1389.

MERGILI M, FRANK B, FISCHER JT, HUGGEL C & PUDASAINI S. 2018b. Computational experiments on the 1962 and 1970 landslide events at Huascaran (Peru) with r.avaflow: lessons learned for predictive mass flow simulations. Geomorphology 322: 15-28.

NARANJO BEDOYA K, ARISTIZÁBAL GIRALDO EV & MORALES RODELO JA. 2019. Influencia del ENSO en la variabilidad espacial y temporal de la ocurrencia de movimientos en masa detonados por lluvias en la región Andina. Ingeniería y Ciencia 15(29): 11-42.

NASA - NATIONAL AERONAUTICS AND SPACE ADMINISTRATION. 2020. Global Landslide Catalog. NASA. Available from: https://catalog.data.gov/dataset/global-landslide-catalog-export. Last access: June 2021.

PENG JB, FAN ZJ, WU D, HUANG QB, WANG QY, ZHUANG JQ & CHE WY. 2019. Landslides triggered by excavation in the loess plateau of China: A case study of Middle Pleistocene loess slopes. J Asian Earth Sci 171: 246-258.

PINEDA MC, MARTINEZ-CASASNOVAS JA & VILORIA J. 2016. Relationship between changes of vegetation cover and landslides ocurrency in mountain ranges of North-central Venezuela. Interciencia 41(3): 190-197.

PLANET TEAM. 2019. Planet Application Program Interface: In Space for Life on Earth. San Francisco, CA. https://api.planet.com. Last access: June 2021.

ROMERO CC, BAIGORRIA GA & STROOSNIJDER L. 2007. Changes of erosive rainfall for El Niño and La Niña years in the northern Andean highlands of Peru. Clim Change 85(3-4): 343-356. https://doi.org/10.1007/s10584-007-9301-0.

RUNYAN CW & D'ODORICO P. 2014. Bistable dynamics between forest removal and landslide occurrence. Water Resour Res 50(2): 1112-1130.

SIDLE RC, FURUICHI T & KONO Y. 2011. Unprecedented rates of landslide and surface erosion along a newly constructed road in Yunnan, China. Nat Hazards 57(2): 313-326.

STARK TD, ARELLANO WD, HILLMAN RP, HUGHES RM, JOYAL N & HILLEBRANDT D. 2005. Effect of toe excavation on a deep bedrock landslide. J Perform Constr 19(3): 244-255.

STUMPF A & KERLE N. 2011. Object-oriented mapping of landslides using Random Forests. Remote Sens Environ 115: 2564-2577.

SUDMEIER-RIEUX K, MCADOO BG, DEVKOTA S, RAJBHANDARI PCL, HOWELL J & SHARMA S. 2019. Invited perspectives: Mountain roads in Nepal at a new crossroads. Nat Hazards Earth Syst Sci 19(3): 655-660.

SWANSON FJ & DRYNESS CT. 1975. Impact of clear-cutting and road construction on soil erosion by landslides in Western Cascade Range, Oregon. Geology 3(7): 393-396.

TACCONI-STEFANELLI C, VILÍMEK V, EMMER A & CATANI F. 2018. Morphological analysis and features of the landslide dams in the Cordillera Blanca, Peru. Landslides 15(3): 507-521.

TAKAHASHI K, MOSQUERA VÁSQUEZ KA & REUPO VÉLEZ JA. 2014. El Índice Costero El Niño (ICEN): historia y actualización. In Repositorio institucional - IGP. Retrieved from Instituto Geofísico del Perú website: http://www.cpc.ncep.noaa.gov/data/indices/ersst3b.nino.mth.81-10.

TAYLOR FE, TAROLLI P & MALAMUD BD. 2020. Preface: Landslide–transport network interactions. Nat Hazards Earth Syst Sci 20: 2585-2590.

VILÍMEK V, KLIMEŠ J & TORRES ZAPATA M. 2016. Reassessment of the development and hazard of the Rampac Grande landslide, Cordillera Negra, Peru. Geoenvironmental Disasters 3: 5.

VUILLE M & KEIMIG F. 2004. Interannual Variability of Summertime Convective Cloudiness and Precipitation in the Central Andes Derived from ISCCP-B3 Data. J Clim 17(17): 3334-3348.

WANG HB, LI XC, MI ZJ, YANG LY & YANG ZL. 2011. Research on formation evolution mechanism of waste dumps landslides on loess foundation. Rock and Soil Mechanics 32(12): 3672-3678.

WANG WP, YIN YP, ZHU SN, WANG LC, ZHANG N & ZHAO RX. 2020. Investigation and numerical modeling of the overloading-induced catastrophic rockslide avalanche in Baige, Tibet, China. Bull Eng Geol 79(4): 1765-1779.

SUPPLEMENTARY MATERIAL

Table SI

How to cite
EMMER A, HÖLBLING D, ABAD L, ŠTĚPÁNEK P, ZAHRADNÍČEK P & EMMEROVÁ I. 2022. Landslides associated with recent road constructions in the Río Lucma catchment, eastern Cordillera Blanca, Peru. An Acad Bras Cienc 94: e20211352. DOI 10.1590/0001-3765202220211352.

Manuscript received on October 7, 2021;
accepted for publication on January 30, 2022

ADAM EMMER[1,3]
https://orcid.org/0000-0002-8268-990X

DANIEL HÖLBLING[2]
https://orcid.org/0000-0001-9282-8072

LORENA ABAD[2]
https://orcid.org/0000-0003-0554-734X

PETR ŠTĚPÁNEK[3]
https://orcid.org/0000-0001-5000-8180

PAVEL ZAHRADNÍČEK[3]
https://orcid.org/0000-0002-4307-0936

ILONA EMMEROVÁ[4]
https://orcid.org/0000-0002-3738-2140

[1]University of Graz, Institute of Geography and Regional Science, Heinrichstraße 36, 8010 Graz, Austria

[2]University of Salzburg, Department of Geoinformatics - Z_GIS, Schillerstrasse 30, 5020 Salzburg, Austria

[3]The Czech Academy of Sciences, Global Change Research Institute (CzechGlobe), Bělidla 986/4a, 603 00 Brno, Czechia

[4]Independent researcher, Makotřasy 26, 273 54 Makotřasy, Czechia

Correspondence to: **Adam Emmer**
E-mail: aemmer@seznam.cz or adam.emmer@uni-graz.at

Author contributions

AE designed the study, conducted the field campaign with IE, and prepared the manual inventory of landslides. DH and LA processed remotely sensed images and employed OBIA for landslide mapping. LA, PZ and PŠ discussed available and suitable rainfall data. LA processed rainfall data and conducted the rainfall analysis. All the authors discussed the content, developed the general framework, contributed to the writing process and approved the final version of the manuscript.